Title

GENERALIZED ANALYSIS OF PHASE-SENSITIVE DETECTION CIRCUIT OPERATING CHARACTERISTICS AT THE SIGNAL DETECTION IN THE PRESENCE OF NOISE

Authors

Branko
Leskorar

Publication Date

1971-03-01

To be submitted for publication

UCRL-20252
Preprint c.2

GENERALIZED ANALYSIS OF PHASE-SENSITIVE DETECTION CIRCUIT OPERATING CHARACTERISTICS AT THE SIGNAL DETECTION IN THE PRESENCE OF NOISE

Branko Leskovar

March 1971

AEC Contract No. W-7405-eng-48

LAWRENCE RADIATION LABORATORY
UNIVERSITY of CALIFORNIA BERKELEY

Generalized Analysis of Phase-Sensitive Detection Circuit Operating Characteristics at the Signal Detection in the Presence of Noise

Branko Leskovar
Lawrence Radiation Laboratory
University of California
Berkeley, California

March 1971

Abstract

This paper presents **a new generalized analysis of operating characteristics** of phase-sensitive detector circuits, assuming that the input signal and the reference wave are in the presence of independent, stationary, and additive Gaussian noise. By means of computer-aided analysis, using high-density discrete value calculations, the generalized criteria are determined for the detector optimum operating conditions and for minimization of the detector characteristics essential nonlinearities. The results of the analysis are given in a normalized form and can be directly applied to evaluate in detail the detector circuit performance and characteristics essential nonlinearities over a wide dynamic range of operating conditions. Furthermore, particular emphasis is laid on the determination of optimum detector circuit operating conditions in contemporary instrumentation systems.

Introduction

The process of phase-sensitive detection often finds its application as an important method of signal processing in instrumentation systems of a multitude of research areas, such as experimental physics [1], [2], radio astronomy [3], nuclear magnetic resonance [4] - [6], electron spin resonance [7], cyclotron resonance [8], automatic control systems [9], and phase-lock techniques [10]. Previous analyses of phase-sensitive detection circuits at the signal detection in the presence of noise [11] - [14] have been based on the assumption that the additive noise is nonexistent in the detector reference channel. However, in contemporary instrumentation and phase-lock systems, where a significant amount of noise can be present in the reference channel, the generalized analysis of detector operating characteristics is needed, which will include the reference channel noise. Results from such an analysis could be employed to optimize the instrumentation systems, as well as to predict accurately their performances. Based on previously mentioned works [12], further effort has been expanded by means of computer-aided analysis to include the noise contribution in the reference channel and to calculate the detector characteristics and its essential nonlinearities in general forms over a wide dynamic range of operating conditions.

Derivation of the Detector Operating Characteristics

The generalized phase-sensitive detection circuit under consideration is shown in Fig. 1. The circuit input signal consists of an input sinusoidal signal $s^*(t) = S^* \cos \omega_0 t$ superimposed on a stationary broad-band Gaussian noise $n_s^*(t)$. After time-invariant linear narrow-band filtering, the sum $s_i(t) = s(t) + n_s t$ is applied to the balanced phase-sensitive detector. The presence of the input signal in the narrow-band Gaussian noise at the detector signal input is characterized by the input signal-to-noise ratio $x_s = S/N_s$, where S is the amplitude of the sinusoidal signal and N_s is the root-mean-square value of the narrow-band noise in the signal channel. The detector reference input consists of a reference wave $r^*(t) = R^* \cos (\omega_0 t + \psi)$ superimposed on a broad-band Gaussian noise $n_r^*(t)$. ψ is the phase angle between the input signal and the reference wave. Again, after filtering, the sum $r_i(t) = r(t) + n_r(t)$ is applied to the detector. The presence of the reference wave in the narrow-band noise is described by the reference wave-to-noise ratio $\mu_r = R/N_r$, where R is the amplitude of the filtered reference wave and N_r is the root-mean-square value of the reference channel narrow-band noise.

The conventional phase-sensitive detector usually consists of a phase-splitter, two adders, two envelope detectors, and a differential circuit. After narrow-band filtering, combined input signal $s_i(t)$ is applied to the phase splitter. Two voltages $s_A(t)$ are available from the splitter, with amplitudes that randomly change. They are in anti-phase over the frequency range of interest. Two adders perform addition of $s_A(t)$ and $s_B(t)$ with detector reference input $r_i(t)$. The addition circuits are followed by envelope detectors. The envelope detector outputs S_A and S_B are subtracted in differential circuit. The dc output of varying amplitude from differential circuit represents the output signal S_o of the detector.

If $n_s(t)$ and $n_r(t)$ are independent Gaussian processes, according to [12] and [13], the narrow-band Gaussian noises at the signal and reference inputs are represented by equations

$$n_s(t) = n_{sp}(t) \cos \omega_o t - n_{sq} \sin \omega_o t \tag{1}$$

and

$$n_r(t) = n_{rp}(t) \cos \omega_o t - n_{rq} \sin \omega_o t \tag{2}$$

respectively.

$n_{sp}(t)$, $n_{sq}(t)$, $n_{rp}(t)$, and $n_{rq}(t)$ are independent Gaussian processes with zero mean, and standard deviations N_s and N_r. Consequently, after additions, the input wave $s_A(t)$ in the first envelope detector can be written in the form

$$s_A(t) = \xi(t) \cos \omega_o t - \eta(t) \sin \omega_o t. \tag{3}$$

The terms $\xi(t) = S + R \cos \psi + n_{sp}(t) + n_{rq}(t)$ and $n(t) = R \sin \psi + n_{sq}(t) + n_{rq}(t)$ are normally distributed variables with the standard deviation $\left(N_r^2 + N_s^2\right)^{1/2}$ and the mean values $\overline{\xi} = S + R \cos \psi$, and $\overline{\xi} = R \sin \psi$.

Equation (3) can be expressed in terms of an envelope and phase in an equivalent form

$$s_A(t) = S_{RA}(t) \cos [\omega_o t + \phi(t)] \tag{4}$$

where $f_o = \omega_o/2\pi$ is the midband frequency of the narrow-band noise equal to the frequency of $s^*(t)$ and $r^*(t)$. The probability density function of $s_A(t)$ is given by equation

$$q(S_{RA}) = \frac{S_{RA}}{N_r^2 + N_s^2} \exp - \left[\frac{S_{RA}^2}{2\left(N_r^2 + N_s^2\right)} + v(x_s, \mu_r, \psi, n) \right]$$

$$\times I_o \left[\frac{S_{RA}}{\left(N_r^2 + N_s^2\right)^{1/2}} v^*(x_s, \mu_r, \psi, n) \right] \tag{5}$$

where $S_{RA} \geq o$, and $I_o \left[S_{RA} v^*(x_s, \mu_r, \psi, n)/\left(N_r^2 + N_s^2\right)^{1/2} \right]$ denotes the Bessel function of zero order with the imaginary argument. The functions $v(x_s, \mu_r, \psi, n)$ and $v^*(x_s, \mu_r, \psi, n)$ are defined by

$$v(x_s, \mu_r, \psi, n) = \frac{\mu_r^2}{2(1 + n^2)} + \frac{x_s^2}{2(1 + n^{-2})} + \frac{\mu_r x_s}{n + n^{-1}} \cos \psi \tag{6}$$

and $v^*(x_s, \mu_r, \psi, n) = [v(x_s, \mu_r, \psi, n)]^{1/2}$ (7)

where n is the signal channel noise-to-reference channel noise ratio $n = N_s/N_r$.

The envelope mean value, denoted by $\overline{S_{RA}}$, is given by the first moment of the distribution of the random variable S_{RA}:

$$\overline{S_{RA}} = \int_o^\infty S_{RA} q(S_{RA}) dS_{RA} = \left(N_r^2 + N_s^2\right)^{1/2} \left(\frac{\pi}{2}\right)^{1/2} u_\alpha[v(x_s, \mu_r, \psi, n)]. \tag{8}$$

The function $u_\alpha[v(x_s, \mu_r, \psi, n)]$ is given by

$$u_\alpha[v(x_s, \mu_r, \psi, n)] = {}_1F_1\left\{-\frac{1}{2};\ 1;\ -\left[\frac{\mu_r^2}{2(1+n^2)} + \frac{x_s^2}{2(1+n^{-2})} + \frac{\mu_r x_s}{n+n^{-1}}\cos\psi\right]\right\} \tag{9}$$

where ${}_1F_1$ denotes the confluent hypergeometric function [15] defined by

$${}_1F_1(a;\ b;\ \pm p) = \frac{a}{b}\cdot\frac{(\pm p)}{1!} + \frac{a(a+1)}{b(b+1)}\frac{(\pm p)^2}{2!} + \frac{a(a+1)(a+2)}{b(b+1)(b+2)}\frac{(\pm p)^3}{3!} + \ldots\ . \tag{10}$$

The dc output of varying amplitude from the first envelope detector is given by the relation

$$S_A = \eta_d\overline{S_{RA}} = \eta_d\left(\frac{\pi}{2}\right)^{1/2}\left(N_r^2 + N_s^2\right)^{1/2}\ u_\alpha[v(x_s, \mu_r, \psi, n)] \tag{11}$$

where η_d is the detection efficiency of the envelope detector.

Similarly, the dc output from the second envelope detector is given by

$$S_B = \eta_d\overline{S_{RB}} = \eta_d\left(\frac{\pi}{2}\right)^{1/2}\left(N_r^2 + N_s^2\right)^{1/2}\ y_\beta[t(x_s, \mu_r, \psi, n)] \tag{12}$$

where function $y_\beta[t(x_s, \mu_r, \psi, n)]$ is defined by the relation

$$y_\beta(t(x_s, \mu_r, \psi, n)] = {}_1F_1\left\{-\frac{1}{2};\ 1;\ -\left[\frac{\mu_r^2}{2(1+n^2)} + \frac{x_s^2}{2(1+n^{-2})} - \frac{\mu_r x_s}{n+n^{-1}}\cos\psi\right]\right\}\ . \tag{13}$$

The envelope detector outputs S_A and S_B are subtracted in differential circuit. The differential circuit dc output of varying amplitude represents the output signal S_o of the detector. It can be expressed in normalized form as:

$$\frac{S_o}{\eta_d\left(N_r^2 + N_s^2\right)^{1/2}} = \left(\frac{\pi}{2}\right)^{1/2}\left\{u_\alpha[v(x_s, \mu_r, \psi, n)] - y_\beta[t(x_s, \mu_r, \psi, n)]\right\} \tag{14}$$

where functions $u_\alpha[v(x_s, \mu_r, \psi, n)]$ and $y_\beta(t(x_s, \mu_r, \psi, n)]$ are given by expressions (9) and (13).

Equation (14) represents the generalized and normalized form of the phase-sensitive detector operating characteristics, where both the input signal and the reference wave have been corrupted by the statistically independent additive Gaussian noise.

Detector characteristics and their essential nonlinearities relating to the input signal-to-noise ratio

By means of a digital computer, the normalized detector characteristics as a function of the input signal-to-noise ratio are calculated and plotted as shown in Figs. 2-4, for the phase angle $\psi_A = 2m\pi$, where $m = 0, 1, 2, \ldots$. High accuracy numerical calculations of the confluent hypergeometric functions in (14) are performed by methods as given in [13]. Since the applications of the phase-sensitive detection demand a detailed evaluation of detector characteristics over a wide dynamic range of operating conditions and significant parameters, the signal channel noise-to-reference channel noise ratios n of 10^{-3}, 1, 10^{3}, and the reference wave-to-noise ratios μ_r of 10^{-2}, 10^{-1}, 1, 10, 10^{2}, 10^{3}, and 10^{4} are chosen as parameters. The following conclusions and observations can be directly made from (14) and Figs. 2-4.

1. When the functions $v(x_s, \mu_r, \psi, n) = \mu_r^2/2(1 + n^2) + x_s^2/2(1 + n^{-2}) + 2\mu_r x_s \cos\psi/n + n^{-1}$ and $t(x_s, \mu_r, \psi, n) = \mu_r^2/2(1 + n^2) + x_s^2/2(1 + n^{-2}) - 2\mu_r x_s \cos\psi/n + n^{-1}$ are much less than one, only the first two terms can be taken into consideration in the expansion (10) of the confluent hypergeometric function. By substituting (10) into (14) it follows that

$$\frac{S_o}{\eta_d\left(N_r^2 + N_x^2\right)^{1/2}} \approx \left(\frac{\pi}{2}\right)^{1/2} \frac{\mu_r x_s}{n + n^{-1}} \cos\psi . \qquad (15)$$

The approximation error is less than 0.3% for the function values $v(x_s, \mu_r, \psi, n) \leq 0.1$ and $t(x_s, \mu_r, \psi, n) \leq 0.1$. The normalized detector output signal $S_o/\eta_d\left(N_r^2\right)^{1/2}$ is in the first approximation a linear function of the input signal-to-noise ratio x_s and the reference wave-to-noise ratio μ_r.

2. In the case when the functions $v(x_s, \mu_r, \psi, n)$ and $t(x_s, \mu_r, \psi, n)$ are much larger than one, the asymptotic expansion of the confluent hypergeometric function given in [13] can be used. Consequently, eq. [14] is reduced to:

$$\frac{S_o}{\eta_d\left(N_r^2 + N_s^2\right)^{1/2}} \approx [2v(x_s, \mu_r, \psi, n)]^{1/2} + \frac{1}{2\sqrt{2}} [v(x_s, \mu_r, \psi, n)]^{-1/2}$$

$$- [2t(x_s, \mu_r, \psi, n)]^{1/2} - \frac{1}{2\sqrt{2}} [t(x_s, \mu_r, \psi, n)]^{1/2}. \tag{16}$$

Furthermore, if $S>>R$, substitution of $n = N_s/N_r$, $\mu_r = R/N_r$, $x_s = S/N_s$, and approximations $(S^2 + 2RS\cos\psi)^{1/2} \approx S + R\cos\psi$ and $(S^2 - 2RS\cos\psi)^{1/2} \approx S - R\cos\psi$ into eq. (16) finally give for the detector output

$$S_o \approx 2\eta_d R\cos\psi . \tag{17}$$

The output signal amplitude in this case is approximately a linear function of the reference wave amplitude. When $S<<R$, by similar considerations it follows that the output signal amplitude is approximately a linear function of the input signal amplitude, or

$$S_o \approx 2\eta_d S\cos\psi . \tag{18}$$

The output signal practically does not depend on the amplitude of the reference wave. Conclusions expressed by eqs. (17) and (18) are in complete agreement with previously published less generalized results [13].

3. Generally, there is a strong dependence of the normalized detector output signal upon μ_r and n, as can be seen from Figs. 2-4. For $n = 10^{-3}$,

the amount of $S_o/\eta_d\left(N_r^2 + N_s^2\right)^{1/2} \approx S_o/10^3\eta_d N_s$. Curves in Fig. 2 show that for $x_s \leq 10^3$, and $\mu_r = 10^{-2}, 10^{-1}, 1$, the detector output-to-signal channel noise ratio $S_o/\eta_d N_s$ is in the first approximation a linear function of the input signal-to-noise ratio. When $x_s \gg 10^3$, the amount of $S_o/\eta_d N_s$ approaches a constant value and in fact does not depend on x_s. This saturation level of $S_o/\eta_d N_s$ depends strongly upon the μ_r amount. If μ_r has a constant value c, the limit of the output signal-to-noise ratio as x_s tends to infinity is

$$\lim_{x_s \to \infty} (S_o/\eta_d N_s)_{n = 10^{-3}} = 2 \times 10^3 \quad . \tag{19}$$

However, there is approximately the same corner value of the input signal-to-noise ratio $x_{sc} \approx 1.7 \times 10^3$ for all amounts of μ_r, if condition $\mu_r \leq 1$ is satisfied. Where $\mu_r \geq 1$, the amounts of x_{sc} shift to higher values, having a particular amount for a given μ_r.

For $n = 1$, the value of $S_o/\eta_d\left(N_r^2 + N_s^2\right)^{1/2} = S_o/\sqrt{2}\eta_d N_s$. Curves in Fig. 3 show that for $x_s \leq 1$, and $\mu_r = 10^{-2}, 10^{-1}, 1$, the detector output-to-signal channel noise ratio $S_o/\eta_d N_s$ is approximately a linear function of the input signal-to-noise ratio. Again, if μ_r has a constant value c, the limit of the output signal-to-noise ratio as x_s tends to infinity is

$$\lim_{x_s \to \infty} (S_o/\eta_d N_s)_{n = 1} = \sqrt{2}c \ . \tag{20}$$

The corner input signal-to-noise ratio $x_{sc} \approx 2.4$ for $\mu_r \leq 1$. When $\mu_r \geq 1$, the value of $x_{sc} \approx \mu_r$.

For $n = 10^3$, the amount of $S_o/\eta_d\left(N_r^2 + N_s^2\right)^{1/2} \approx S_o/\eta_d N_s$. In this case only curves for $\mu_r = 10, 10^2, 10^3, 10^4$ are plotted inside a dynamic range of x_s from 10^{-2} to 10^4 and $S_o/\eta_d N_s$ from 10^{-2} to 10^4, as shown in Fig. 4. The limit of the output signal-to-noise ratio, if μ_r has a constant value of c, as x_s tends to infinity is

$$\lim_{x_s \to \infty} (S_o/\eta_d N_s)_{n = 10^3} = 2 \times 10^{-3} c \quad . \tag{21}$$

Furthermore, for $\mu_r \leq 1$ the corner value of the input signal-to-noise ratio $x_{sc} \approx 1.7$. If $\mu_r \geq 1$, the values of $x_{sc} \approx 10^3 \mu_r$.

When the phase angle $\psi_B = (2m + 1)\pi/2$, the detector output equal zero for any amount of x_s, μ_r, and n, as can be seen from (14). If the phase angle $\psi_c = (2m + 1)\pi$, the same conclusions are valid for the normalized detector output as in the previously considered case for $\psi_A = 2m\pi$, but the sign of the detector output is negative.

In addition to the above given considerations, the essential nonlinearity $N_A^*(x_s)$ of the detector characteristics has been determined as a function of x_s for the phase angle $\psi_A = 2m\pi$. The nonlinearity $N_A^*(x_s)$ is evaluated from the extent of detector characteristic departure from the tangent drawn to the characteristic at point $x_s = o$. The tangent slope to the detector characteristic at point $x_s = o$ is given by the partial differentiation of function (14) with respect to x_s. Differentiation gives the result:

$$\frac{\delta}{\delta x_s} \left[\frac{S_o}{\eta_d \left(N_r^2 + N_s^2\right)^{1/2}} \right] = \frac{1}{2}\left(\frac{\pi}{2}\right)^{1/2} \frac{1}{N_s + \frac{N_r^2}{N_s}} \left\{ (S + R \cos \psi) s_\alpha [v(x_s, \mu_r, \psi, n)] - \right.$$

$$\left. - (S - R \cos \psi) m_\beta [t(x_s, \mu_r, \psi, n)] \right\} \tag{22}$$

where functions $s_\alpha[v(x_s, \mu_r, \psi, n)]$ and $m_\beta[t(x_s, \mu_r, \psi, n)]$ are defined by:

$$s_\alpha[v(x_s, \mu_r, \psi, n)] = {}_1F_1 \left\{ \frac{1}{2}; 2; - \left[\frac{\mu_r^2}{2(1 + n^2)} + \frac{x_s^2}{2(1 + n^{-2})} + \frac{\mu_r x_s}{n + n^{-1}} \cos \psi \right] \right\} \tag{23}$$

$$m_\beta[t(x_s, \mu_r, \psi, n)] = {}_1F_1 \left\{ \frac{1}{2};\ 2;\ - \left[\frac{\mu_r^2}{2(1+n^2)} + \frac{x_s^2}{2(1+n^{-2})} - \frac{\mu_r x_s}{n+n^{-1}} \cos\psi \right] \right\}. \tag{24}$$

The equation of the tangent to the detector characteristic at point $x_s = o$, with $\psi_A = 2m\pi$ is

$$u^*(x_s) = \left(\frac{\pi}{2}\right)^{1/2} \frac{SR}{N_s^2 + N_r^2}\ \kappa^*(\mu_r, n) \tag{25}$$

where

$$\kappa^*(\mu_r, n) = {}_1F_1 \left[\frac{1}{2};\ 2;\ - \frac{\mu_r^2}{2(1+n^2)} \right]. \tag{26}$$

The detector output for the phase angle ψ_A is given from equation (14) in the form:

$$y^*(x_s) = \left(\frac{\pi}{2}\right)^{1/2} \left\{ \phi^*[f(x_s, \mu_r, n)] - z^*[h(x_s, \mu_r, n)] \right\} \tag{27}$$

where functions $\phi^*[f(x_s, \mu_r, n)]$ and $z^*[h(x_s, \mu_r, n)]$ are given by

$$\phi^*[f(x_s, \mu_r, n)] = {}_1F_1 \left\{ -\frac{1}{2};\ 1;\ - \left[\frac{\mu_r^2}{2(1+n^2)} + \frac{x_s^2}{2(1+n^{-2})} + \frac{\mu_r x_s}{n+n^{-1}} \right] \right\} \tag{28}$$

$$z^*[h(x_s, \mu_r, n)] = {}_1F_1 \left\{ -\frac{1}{2};\ 1;\ - \left[\frac{\mu_r^2}{2(1+n^2)} + \frac{x_s^2}{2(1+n^{-2})} - \frac{\mu_r x_s}{n+n^{-1}} \right] \right\}. \tag{29}$$

The essential nonlinearity $N_A^*(x_s)$ of the detector characteristics relating to the input signal-to-noise ratio is directly given by the expression

$$N_A^*(x_s) = \frac{u^*(x_s) - y^*(x_s)}{u^*(x_s)} = 1 - \gamma^*(x_s, \mu_r, n) \frac{\phi^*[f(x_s, \mu_r, n)] - z^*[h(x_s, \mu_r, n)]}{\kappa^*(\mu_r, n)} \tag{30}$$

where

$$\Upsilon^{*}(x_s, \mu_r, n) = \frac{1}{x_s \mu_r} (n + n^{-1}). \quad (31)$$

By means of a digital computer, the nonlinearity $N_A^*(x_s)$ as a function of x_s with μ and n as parameters is calculated and plotted over a wide range of operating conditions (Figs. 5-6).

Similarly, as in previous considerations concerning the detector characteristics dependence upon μ_r and n, there is a strong dependence of the essential nonlinearity $N_A^*(x_s)$ ratio. It can be seen from Fig. 5 that there are two different groups of curves for $N_A^*(x_s)$. The left-hand group of curves belongs to the case when $n = 10^{-3}$. The right-hand group is for $n = 10^3$. For $n = 10^{-3}$, nonlinearity is plotted for $\mu_r = 10^{-2}$, 10^{-1}, 1, 5, and 10. For any higher value of μ_r the nonlinearity curves are outside of dynamic range from 10^{-2} to 10^4 for x_s. In general the nonlinearity increases with the increase of the signal-to-noise ratio, for a given μ_r. Also, $N_A^*(x_s)$ decreases by increasing the μ_r/x_s ratio, particularly when $\mu_r \geq 1$. In particular, if the ratio $\mu_r/x_s \leq 10^{-2}$, the nonlinearity $N_A^*(x_s) \lessapprox 0.1\%$. When $\mu_r/x_s \leq 10^{-1}$, the nonlinearity has value $N_A^*(x_s) \lessapprox 0.01\%$. In some cases the increase of μ_r/x_s ratio for one order of magnitude decreases the nonlinearity more than three orders of magnitude, as can be seen by inspection of curves for $\mu_r = 1$, 10, and $x_s = 10^3$. Actually the nonlinearity is even more reduced for larger amounts of x_s, and for the same increase of μ_r/x_s ratio. Generally, the nonlinearity has a small value over a wide dynamic range of x_s. However, if the minimum nonlinearity value is desirable, it is important to optimize the detector operating conditions by choosing the ratio μ_r/x_s as large as possible.

It is also apparent that in the case when the signal channel noise-to-reference channel noise ratio is large, $n = 10^3$, the minimization of the nonlinearity requires a very high value of μ_r/x_s ratio. Specifically, curves show that $\mu_r/x_s = 5.10^3$ for the nonlinearity $N_A^*(x_s) = 0.1\%$, and $x_s = 1$. For $\mu_r = x_s$, and $x \geq 1$, the essential nonlinearity $N_A^*(x_s) \geq 11\%$. This amount is unacceptable for most practical applications. Exceptions are cases where detector nonlinearity is purposely introduced, such as in phase-lock loop systems to improve the system performance. It follows that for this particular case it is very difficult to obtain a satisfactory small value of $N_A^*(x_s)$, because of the general shift of all curves involved to the smaller values of x_s, as well as to the grouping of characteristics for $\mu_r \leq 10^3$.

Curves in Fig. 6 show that for n = 1 the nonlinearity $N_A^*(x_s)$ can be considerably decreased by increasing the ratio μ_r/x_s. For example, increasing μ_r/x_s ratio by one order of magnitude will decrease the nonlinearity by almost three orders of magnitude for $x_s = 1$. Furthermore, the nonlinearity is even more reduced for larger amounts of x_s. It can be seen that for $\mu_r = 10$, increasing μ_r by one order of magnitude decreases the nonlinearity by more than four orders of magnitude. Consequently, the gain in the nonlinearity decrease is larger for larger x_s, for the same increase of μ_r/x_s. However, for purposes of obtaining the largest output signal and a wide dynamic range in wide-band phase sensitive detection application by using solid state components, x_s can be close in value to μ_r. In such an application, essential nonlinearity can have an appreciable value, especially for small μ_r and x_s. With increasing μ_r and x_s the essential nonlinearity is gradually increased, between lines $x_s = 1$ and $x_s = 10$, and after $x_s = 10$ decreased, as can be concluded by comparison of the curves. For the case $\mu_r = x_s$, approximate values of $N_A^*(x_s)$ can be seen from Fig. 6: 5, 7.5, 1, and 0.1% for x_s equals 1, 10, 10^2, and 10^3, respectively. However, if both μ_r and x_s are greater than 10, μ_r always has to be slightly larger than x_s. If this condition is not satisfied, the nonlinearity can reach an unacceptably high value; e.g., for $\mu_r = 100$ and $x_s = 80$ the nonlinearity $\approx 0.0017\%$. On the other hand, for $\mu_r = 100$ and $x_s = 120$, nonlinearity is more than three orders of magnitude larger, more than approximately 18%. This value of $N_A^*(x_s)$ is unacceptable for most practical applications. In general, the nonlinearity deterioration is larger for larger values of both μ_r and x_s under previously mentioned conditions. Consequently, wherever the essential nonlinearity is of prime importance, the maximum x_s value should always be smaller than μ_r, irrespective of other demands than can be imposed on the phase-sensitive detection circuit for other reasons. This is particularly important in applications in which x_s varies in a wide dynamic range. If x_s is only 10% smaller than μ_r, the nonlinearity $N_A^*(x_s)$ can be reduced by more than one order of magnitude; this can be concluded by inspection and comparison of curves for $\mu_r = 10^2, 10^3$, and 10^4.

Detector characteristics and their essential nonlinearities relating to the phase angle between the input signal and reference wave

Detector characteristics as function of phase angle between the input signal and the reference wave ψ with x_s, n, and μ_r as parameters are calculated from (14) and shown in Figs. 7-9. It should be pointed out that the detector output depends strongly upon previously mentioned parameters. In general, for the phase angle in the vicinity of point $\psi_B = (2n + 1)\pi/2$, the detector output is in the first approximation a linear function of x_s, for any amount of x_s, μ_r, and n. If the phase angles approach the point $\psi_{CB} = 2m\pi$, a nonlinear relationship exists between the detector output and ψ. Since the points ψ_B and ψ_C may be equally important for a particular application, the nonlinearity $N_B^*(x_s)$ of detector characteristics relating to the phase angle in the vicinity of ψ_B, and the nonlinearity N_C relating to the phase angle in the vicinity of the point ψ_{CB} are determined, using the same method as before for $N_A^*(x_s)$. The tangent equation to the detector characteristic at point $\psi_B = (2m + 1)\pi/2$ is

$$w^*(\psi) = \left(\frac{\pi}{2}\right)^{1/2} \frac{RS}{N_r^2 + N_s^2} w[f(x_s, \mu_r, n)] \left[\left(\frac{\pi}{2}\right) - \psi\right] \tag{32}$$

where

$$w[f(x_s, \mu_r, n)] = {}_1F_1 \left\{ \frac{1}{2};\ 2;\ -\left[\frac{\mu_r^2}{2(1+n^2)} + \frac{x_s^2}{2(1+n^{-2})} \right] \right\}. \tag{33}$$

The detector output $z^*(\psi)$ is directly given from eq. (14) in the form:

$$z^*(\psi) = \left(\frac{\pi}{2}\right)^{1/2} \left\{ \mu_\alpha[v(x_s, \mu_r, \psi, n)] - y_\beta[t(x_s, \mu_r, \psi, n)] \right\} \tag{34}$$

where functions $\mu_\alpha[v(x_s, \mu_r, \psi, n)]$ and $y_\beta[t(x_s, \mu_r, \psi, n)]$ are given by (9) and (13).

Hence, the essential nonlinearity $N_B^*(\psi)$ of the detector characteristics with respect to the phase angle between the input signal and reference wave is given by equation

$$N_B^*(\psi) = \frac{w^*(\psi) - z^*(\psi)}{w^*(\psi)} = 1 - \delta^*(x_s, \mu_r, \psi, n) \frac{\mu_\alpha[v(x_s, \mu_r, \psi, n)] - y_\beta[t(x_s, \mu_r, \psi, n)]}{w[f(x_s, \mu_r, n)]}. \tag{35}$$

Function $\delta^*(x_s, \mu_r, \psi, n)$ is defined by

$$\delta^*(x_s, \mu_r, \psi, n) = \frac{n + n^{-1}}{\mu_r x_s} \frac{1}{\left(\frac{\pi}{2} - \psi\right)}. \tag{36}$$

In general, the nonlinearity $N_B^*(\psi)$ depends strongly not only upon ψ, but also an x_s, μ_r, and n. To obtain the most information about $N_B^*(\psi)$ and a better insight into nonlinearity behavior with signal-to-noise ratio variation, the nonlinearity is calculated and plotted in Figs. 10 and 11 as a function of x_s, with ψ, μ_r, and n as parameters. Specifically, in Fig. 10, the nonlinearity $N_B^*(x_s)$ is plotted for $n = 10^{-3}$ and 10^3, with the following values of μ_r: 1, 10, 10^3, and 10^4; and the following fixed values of ψ: 0, $\pi/4$, $\pi/3$, $5\pi/12$, $11\pi/24$, $47\pi/96$, and $99\pi/200$. In Fig. 11, $N_B^*(x_s)$ is plotted for n = 1, with the following values of μ_r: 1, 10, 10^2, 10^3, and 10^4; and the same values of ψ as in Fig. 10.

The curves in Fig. 10 show that for $n = 10^{-3}$ and $\mu_r = 1$, the nonlinearity $N_B^*(x_s)$ is practically independent of the input signal-to-noise ratio over a wide dynamic range. Curves have a small minimum at point $x_s \approx 2.5 \times 10^3$. On the other hand, the nonlinearity strong dependence upon the phase angle is readily evident. The maximum nonlinearity $N_B^*(x_s)_{max}$ appears at the point $\psi_B = o$, but its value depends upon x_s and μ_r. There is a more significant minimum of $N_B^*(x_s)$ for $\mu_r = 10$. The minimum nonlinearity $N_B^*(x_s)_{min}$ is approximately a half order of magnitude smaller than its average value for almost any value of ψ. In general, $N_B^*(x_s)_{min}$ is smaller for larger values of ψ. For any higher value of μ_r the minimums of the curves are outside of x_s dynamic range.

Furthermore, in the case for $n = 10^3$, curves in Fig. 10 show that the detector characteristics have a nonlinearity minimum value for $\mu_r = 10^3$ and 10^4. For $\mu_r \leq 10^3$, the value of $N_B^*(x_s)_{min}$ is so small in comparison with the nonlinearity average amount that it is not clearly visible as a minimum.

Figure 11 illustrates the behavior of $N_B^*(x_s)$ for $n = 1$. It can be seen from the given curves that for any phase angle value, the detector characteristics have a nonlinearity minimum amount if μ_r is close in value to x_s, for the total x_s dynamic range of interest.

The nonlinearity $N_C^*(\psi)$ of the detector characteristics relating to phase angles in the vicinity of the possible operating point $\psi_{CB} = 2m\pi$ is determined by a similar method as the nonlinearity $N_B^*(\psi)$. The tangent equation to the detector characteristic at point ψ_{CB} is given from (14) by

$$f^*(\psi) = \left(\frac{\pi}{2}\right)^{1/2} \left\{ \phi^*[f(x_s, \mu_r, n)] - z^*[h(x_s, \mu_r, n)] \right\} \tag{37}$$

where $\phi^*[f(x_s, \mu_r, n)]$ and $z^*[h(x_s, \mu_r, n)]$ are given by eqs. (28) and (29).

The essential nonlinearity $N_C^*(\psi)$ relating to the phase angle between the input signal and reference wave for the operating point $\psi_{CB} = 2m\pi$ is

$$N_C^*(\psi) = \frac{f^*(\psi) - z^*(\psi)}{f^*(\psi)} = 1 - \frac{\mu_\alpha[v(x_s, \mu_r, \psi, n)] - y_\beta[t(x_s, \mu_r, \psi, n)]}{\phi^*[g(x_s, \mu_r, n)] - z^*[h(x_s, \mu_r, n)]} . \tag{38}$$

To obtain the most information about $N_C^*(\psi)$ and a better insight into its behavior with x_s variation, the nonlinearity is calculated and plotted as a function of x_s with ψ, μ_r, and n as parameters in Figs. 12 and 13. In particular, in Fig. 12, the nonlinearity $N_C^*(x_s)$ is plotted for $n = 10^{-3}$ and 10^3 with the following values of μ_r: 1, 10, 10^3, and 10^4; and the following values of ψ: $47\pi/96$, $\pi/4$, $\pi/12$, $\pi/24$, $\pi/48$, $\pi/36$, and $\pi/300$. Furthermore, in Fig. 13, $N_C^*(x_s)$ is plotted for $n = 1$, with the following values of μ_r: 1, 10, 10^2, 10^3, and 10^4; and for the same values of ψ as in Fig. 12.

The curves in Fig. 12 show that nonlinearity $N_C^*(x_s)$ is almost independent of the input signal-to-noise ratio for $n = 10^{-3}$ and $\mu_r = 1$. However, the nonlinearity strongly depends on the phase angle for any value of x_s, μ_r, and n. There is a maximum of $N_C^*(x_s)$ for $\mu_r = 10$. Generally, the maximum nonlinearity $N_C^*(x_s)_{max}$ is approximately a half order of magnitude larger than its average value for almost any value of ψ. For $\mu_r \geq 10$ the maxima of $N_C^*(x_s)$ are outside of x_s dynamic range. When $n = 10^3$, curves in Fig. 12 show that the detector characteristics have a maximum value for $\mu_r = 10^3$ and 10^4.

In the case when $n = 1$, curves in Fig. 13 show that the detector characteristics have a maximum of the nonlinearity $N_C^*(x_s)_{max}$ if μ_r is close in value to x_s. The nonlinearity maximum is approximately one to two orders of magnitude larger than its average value for any value of ψ. In general, in comparison with its average value, $N_C^*(x_s)_{max}$ is larger for larger values of both x_s and μ_r and smaller values of ψ.

Conclusions

The phase-sensitive detection circuit operating characteristics and their essential nonlinearities have been analyzed, assuming that the input signal and the reference wave are in the presence of independent additive Gaussian noise. Analysis shows that the presence of the reference channel noise has a dominant role in the determination of the detector circuit optimum operating conditions. The obtained expression (14) and the curves in Figs. 2-4 and Figs. 7-9 illustrate the behavior of the detector circuit characteristics under different operating conditions, particularly concerning the influence of the signal channel noise-to-reference channel noise ratio n. Furthermore, expression (30) and curves in Figs. 5-6 show the behavior of the essential nonlinearity $N_A^*(x_s)$ of the detector characteristics. It can be seen from Figs. 5-6 that for a fixed phase angle ψ, and given ratio n, the proper choice of μ_r and x_s minimizes the nonlinearity $N_A^*(x_s)$ to an acceptable amount. This is particularly important in a wide dynamic range, wide-band, phase-sensitive detection application using solid state circuit components. In such an application the ratio μ_r is often close in value to the ratio x_s, resulting in a large essential nonlinearity. From expression (35) for the detector characteristics nonlinearity $N_B^*(\psi)$ with respect to phase angle ψ, and from Figs. 10-11, it follows that the proper choice of μ_r for a given n and x_s minimizes the nonlinearity. Any other value of μ_r can be considered a nonoptimum one, although the nonlinearity increase will not be significant for $\mu_r = 1$, and for small amounts of ψ. Finally, from expression (38) and curves in Figs. 12-13, it follows that particular values of μ_r also minimize the nonlinearity $N_C^*(\psi)$. For this purpose it is important to avoid the regions where $N_C^*(x_s)$ curves have maximums. From comparison of $N_B^*(x_s)$ and $N_C^*(x_s)$ curves it can be seen that nonoptimum values of μ_r, x_s, and n have far larger influence on the behavior of the nonlinearity $N_C^*(x_s)$ than on the nonlinearity $N_B^*(x_s)$. In general, the nonoptimum μ_r, x_s, and n values maximally increase the $N_B^*(x_s)$ for approximately a half order of magnitude in the worst case. However, $N_C^*(x_s)$ nonoptimum values of μ_r, x_s, and n increase $N_C^*(x_s)$ for two orders of magnitude. Consequently, the phase angle $\psi_B = (2m + 1)\pi/2$ should be chosen as an operating point wherever possible. In this case significantly smaller nonlinearities for nonoptimum values of μ_r, x_s, and n result in comparison with operating point $\psi_{CB} = 2m\pi$.

Acknowledgment

The author would like to thank Ruth L. Hinkins for computer programming.

Generalized Analysis of Phase-Sensitive Detection Circuit Operating Characteristics at the Signal Detection in the Presence of Noise

Branko Leskovar

Manuscript received ______________________;

Revised ______________________.

Work done under auspices of the U. S. Atomic Energy Commission.

Lawrence Radiation Laboratory
University of California
Berkeley, California

REFERENCES

[1] C. H. Townes and A. L. Schawlow, Microwave Spectroscopy. New York: McGraw-Hill, 1955, pp. 421-424.

[2] L. Marton, "Methods of experimental physics," in Molecular Physics, vol. 3. New York: Academic Press, 1962, pp. 438-440, 482-484, and 666-668.

[3] R. H. Dicke, "The measurement of thermal radiation of microwave frequencies," Rev. Sci. Instr., vol. 17, pp. 268-275, 1946.

[4] A. Abragam, The Principles of Nuclear Magnetism, Oxford University Press, 1960.

[5] H. Primas and H. H. Günthard, "Ein Kernresonanzspektrograph mit hoher Auflösung," Helvetica Physica Acta, vol. 30, pp. 315-330, 1957.

[6] B. Leskovar, W. W. Lattin, "Ring-type phase-sensitive detector in nuclear magnetic resonance sample receiver for Fourier transform spectroscopy," UCRL Report No. 20251, 1971, Lawrence Radiation Laboratory, University of California, Berkeley.

[7] D. J. Ingram, Spectroscopy at Radio and Microwave Frequencies. London: Butterworth Scientific Publications Ltd., 1967.

[8] J. K. Galt, W. A. Yager, F. R. Merritt, B. B. Cetlin, A. D. Brailsford, "Cyclotron absorption in metallic bismuth and its alloys," Physical Review, vol. 114, p. 1396, 1959.

[9] J. G. Truxal, Control Engineers' Handbook. New York: McGraw-Hill, 1958, pp. 6-61 - 6-65.

[10] F. J. Charles, W. C. Lindsey, "Some analytical and experimental phase-locked loop results for low signal-to-noise ratio," Proceedings of the IEEE, vol. 59, no. 9, Sept. 1966, pp. 1152-1166.

[11] W. C. Lindsey, M. K. Simon, "The effect of loop stress on the performance of phase-coherent communication systems," IEEE Transactions on Communication Technology, vol. COM-18, no. 5, 1970.

[12] B. Leskovar, "Phase-sensitive detector nonlinearity at the signal detection in the presence of noise," IEEE Transactions on Instrumentation and Measurement, vol. IM-16, no. 4, pp. 285-294, 1967.

[13] B. Leskovar, "Essential nonlinearity of phase-sensitive detector characteristics," Proceedings of the Sixth Annual Allerton Conference on Circuit and System Theory, Allerton House, Monticello, Illinois, 1968, pp. 122-130. See also IEEE Transactions on Instrumentation and Measurement, vol. IM-18, no. 2, pp. 81-87, 1969.

[14] B. Leskovar, "Generalized criteria of characteristics nonlinearity of phase-sensitive detection systems," Proceedings of the Third Hawaii International Conference on System Sciences, Honolulu, Hawaii, January 1970, pp. 13-16. Also in IEEE Transactions on Instrumentation and Measurement, vol. IM-19, no. 1, pp. 25-27, 1970.

[15] D. Middleton, An Introduction to Statistical Communication Theory. New York: McGraw-Hill, 1960, pp. 1075-1076.

Figure Captions

Fig. 1. Generalized phase-sensitive detection circuit under consideration.

Fig. 2. Detector characteristics as a function of the input signal-to-noise ratio x_s with the reference wave-to-noise ratio μ_r as parameter, and the signal channel noise-to-reference channel noise ratio $n = 10^{-3}$.

Fig. 3. Detector characteristics as a function of the input signal-to-noise ratio with the reference wave-to-noise ratio μ_r as parameter, and the signal channel noise-to-reference channel noise ratio $n = 1$.

Fig. 4. Detector characteristics as a function of the input signal-to-noise ratio x_s with the reference wave-to-noise ratio μ_r as parameter, and the signal channel noise-to-reference channel noise ratio $n = 10^3$.

Fig. 5. Nonlinearity $N_A^*(x_s)$ versus signal-to-noise ratio x_s, with the reference wave-to-noise ratio μ_r as parameter and the signal channel noise-to-reference channel noise ratio $n = 10^{-3}$ and 10^3.

Fig. 6. Nonlinearity $N_A^*(s)$ versus signal-to-noise ratio x_s, with the reference wave-to-noise ratio μ_r as parameter and the signal channel noise-to-reference channel noise ratio $n = 1$.

Fig. 7. Detector characteristics as a function of the phase angle between the input signal and reference wave ψ with the input signal-to-noise ratio x_s as parameter, the reference wave-to-noise ratio $\mu_r = 10^{-2}$ and 10^4, and the signal channel noise-to-reference channel noise ratio $n = 10^{-3}$.

Fig. 8. Detector characteristics as a function of the phase angle between the input signal and reference wave ψ, with the input signal-to-noise ratio x_s as parameter, the reference wave-to-noise ratio $\mu_r = 10^{-2}$ and 10^4, and the signal channel noise-to-reference channel noise ratio $n = 1$.

Figure Captions (cont'd)

Fig. 9. Detector characteristics as a function of the phase angle between the input signal and the reference wave ψ, with the input signal-to-noise ratio x_s as a parameter, the reference wave-to-noise ratio $\mu_r = 10^{-2}$ and 10^4, and the signal channel noise-to-reference channel noise ratio $n = 10^3$.

Fig. 10. Nonlinearity $N_B^*(x_s)$ versus signal-to-noise ratio x_s, with phase angle ψ and the reference wave-to-noise ratio μ_r as parameters for the signal channel noise-to-reference channel noise ratio $n = 10^{-3}$ and 10^3.

Fig. 11. Nonlinearity $N_B^*(x_s)$ versus signal-to-noise ratio x_s, with phase angle ψ and the reference wave-to-noise ratio μ_r as parameters for the signal channel noise-to-reference channel noise ratio $n = 1$.

Fig. 12. Nonlinearity $N_C^*(x_s)$ versus signal-to-noise ratio x_s, with phase angle ψ and the reference wave-to-noise ratio μ_r as parameters, for the signal channel noise-to-reference channel noise ratio $n = 10^{-3}$ and 10^3.

Fig. 13. Nonlinearity $N_C^*(x_s)$ versus signal-to-noise ratio x_s, with the phase angle ψ and the reference wave-to-noise ratio μ_r as parameters, for the signal channel noise-to-reference channel noise ratio $n = 1$.

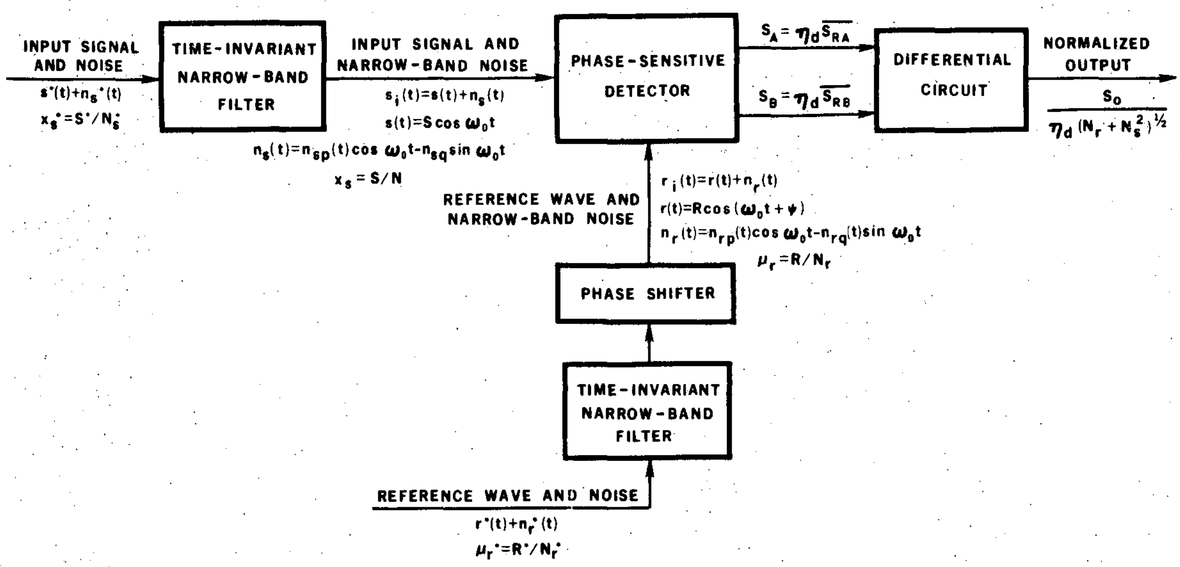

XBL 713-456

Fig. 1

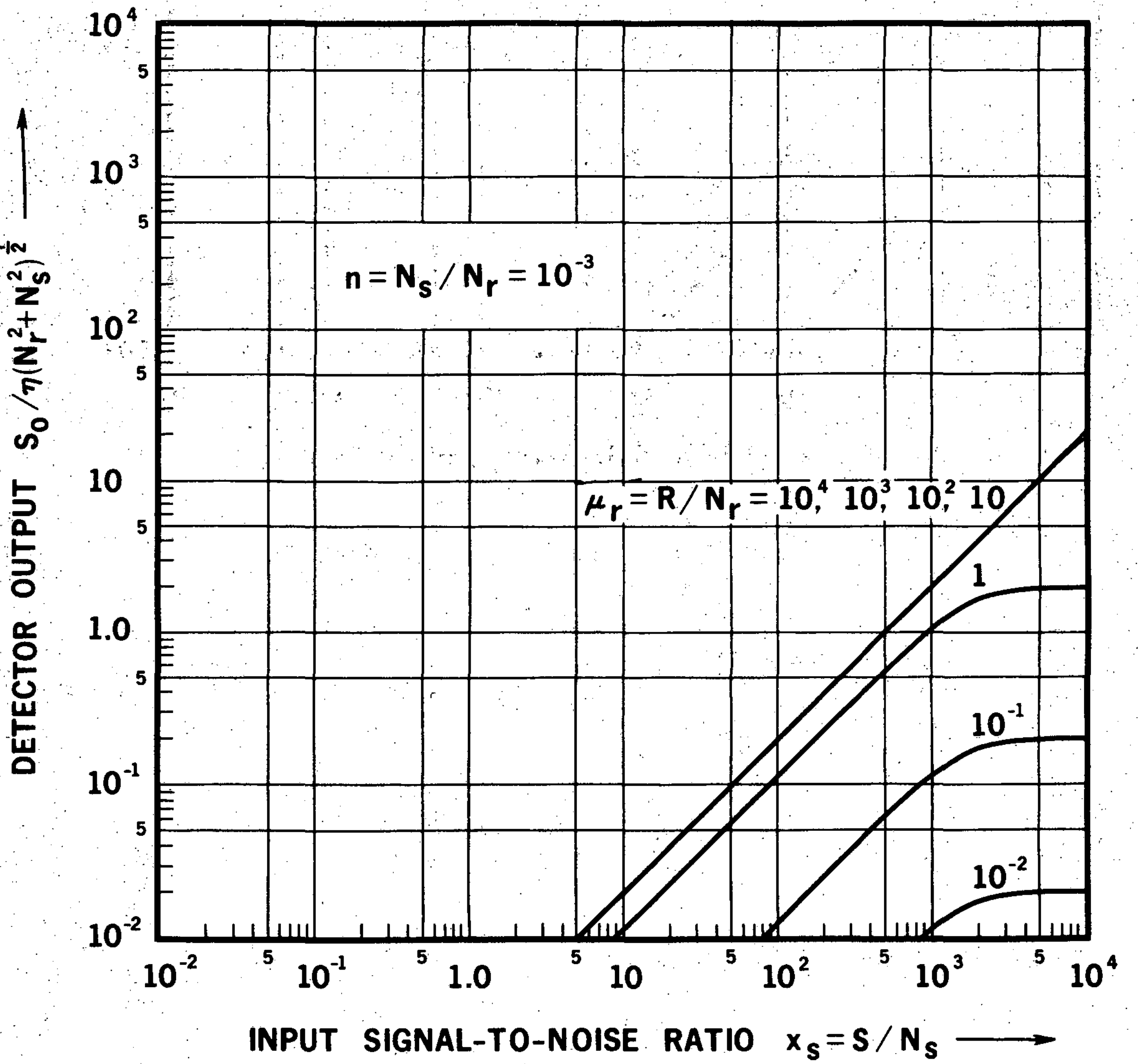

XBL 713-451

Fig. 2

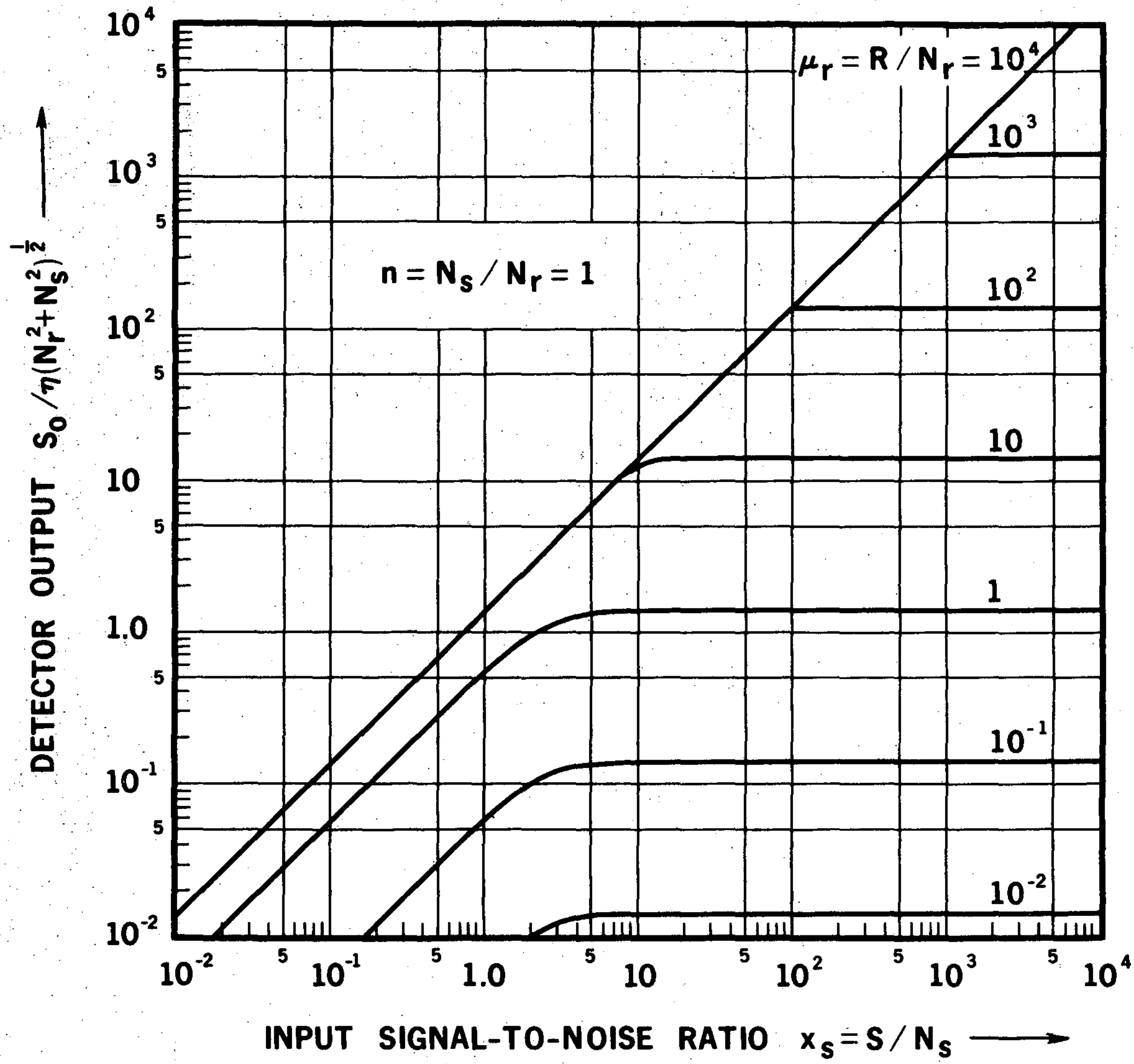

XBL 713-454

Fig. 3

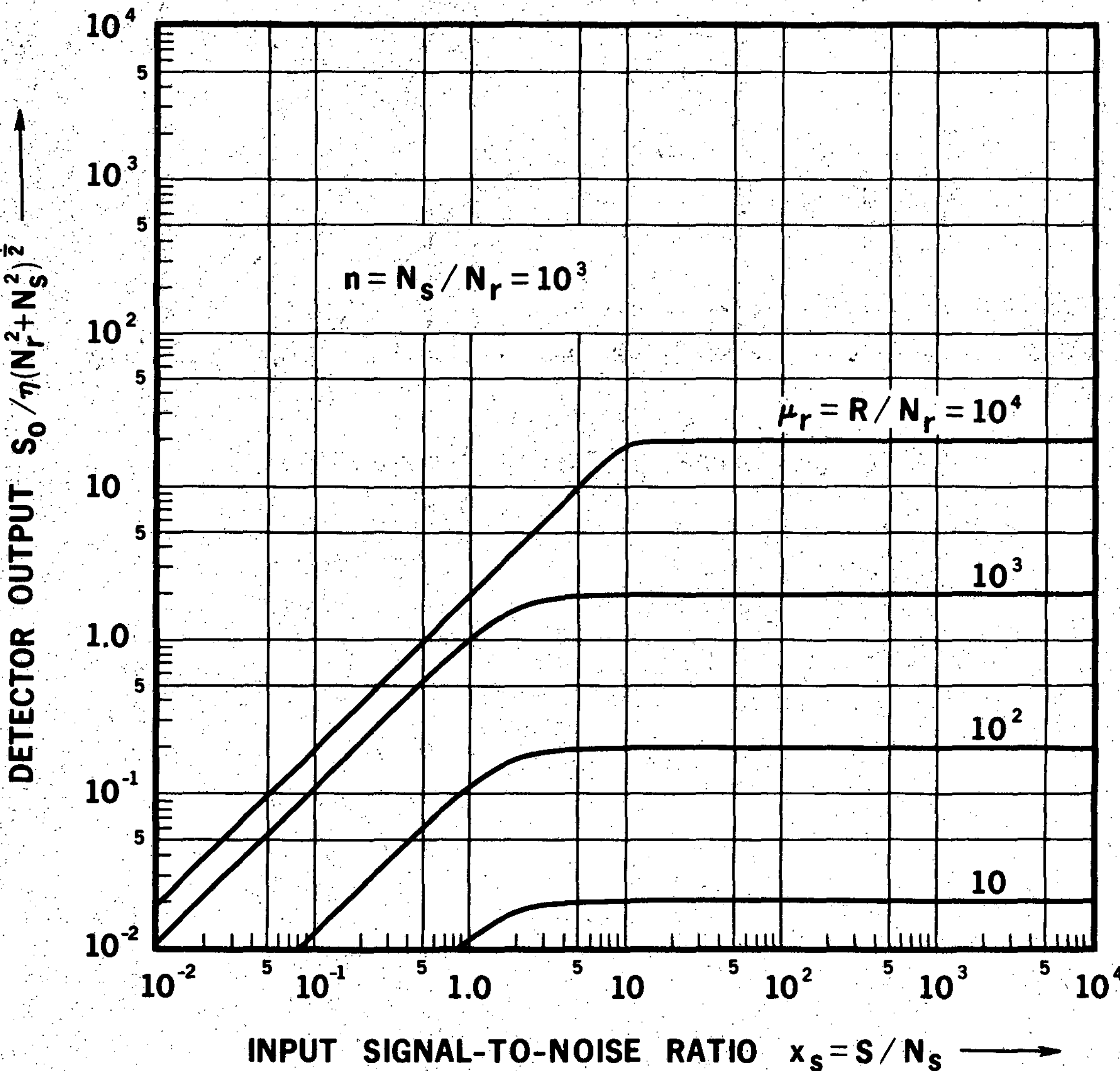

XBL 713-453

Fig. 4

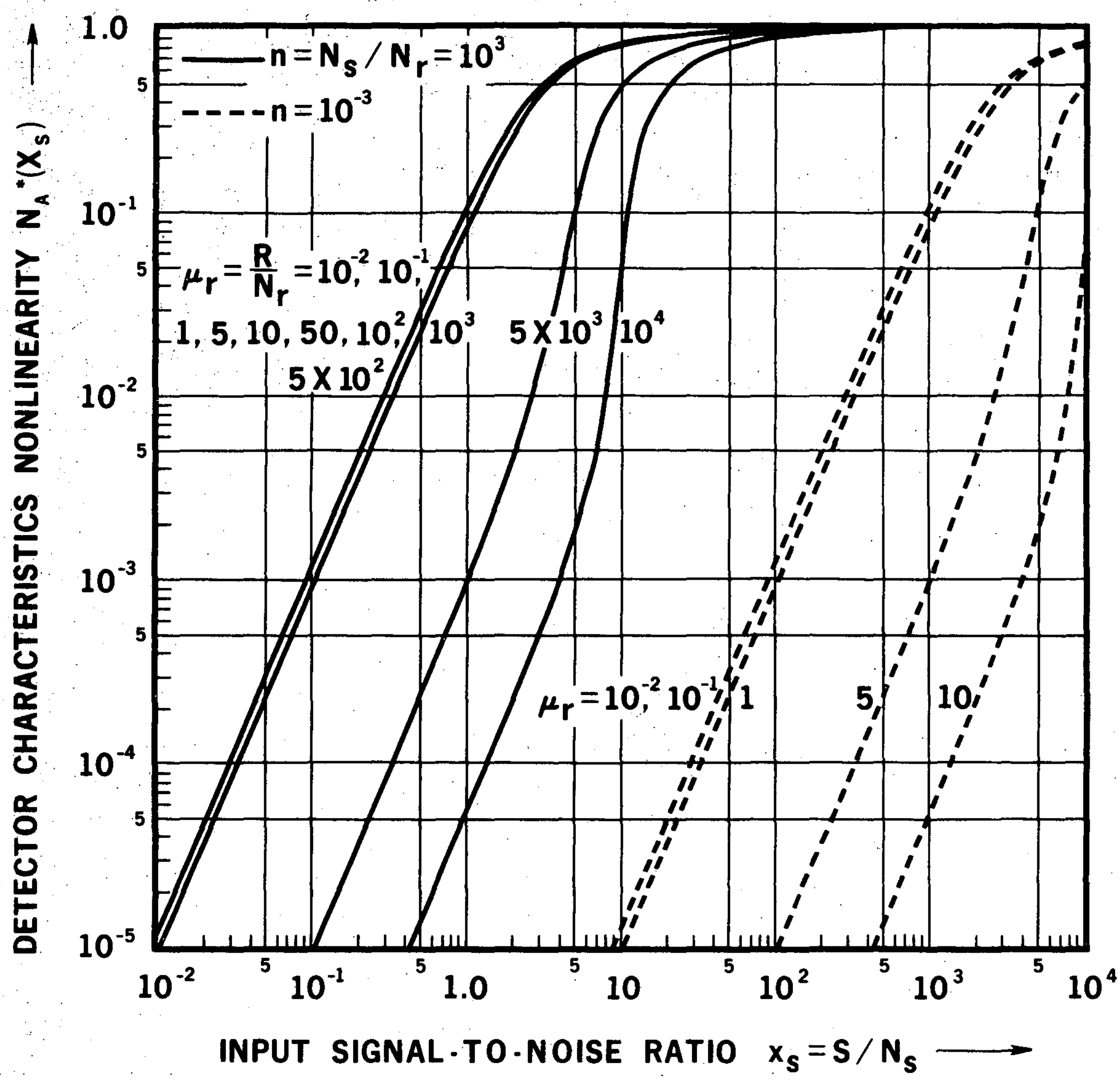

XBL 713-448

Fig. 5

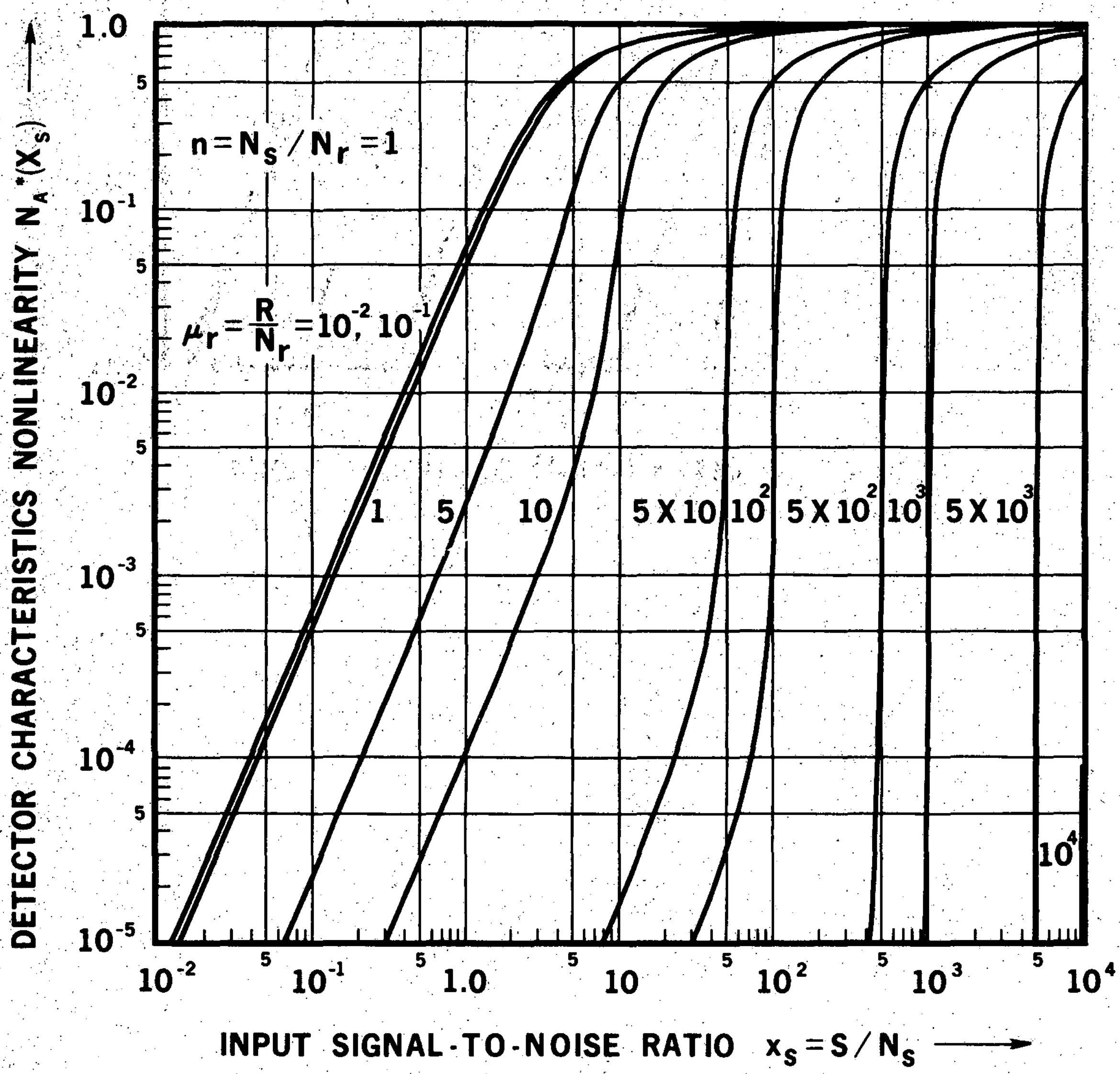

XBL 713-447

Fig. 6

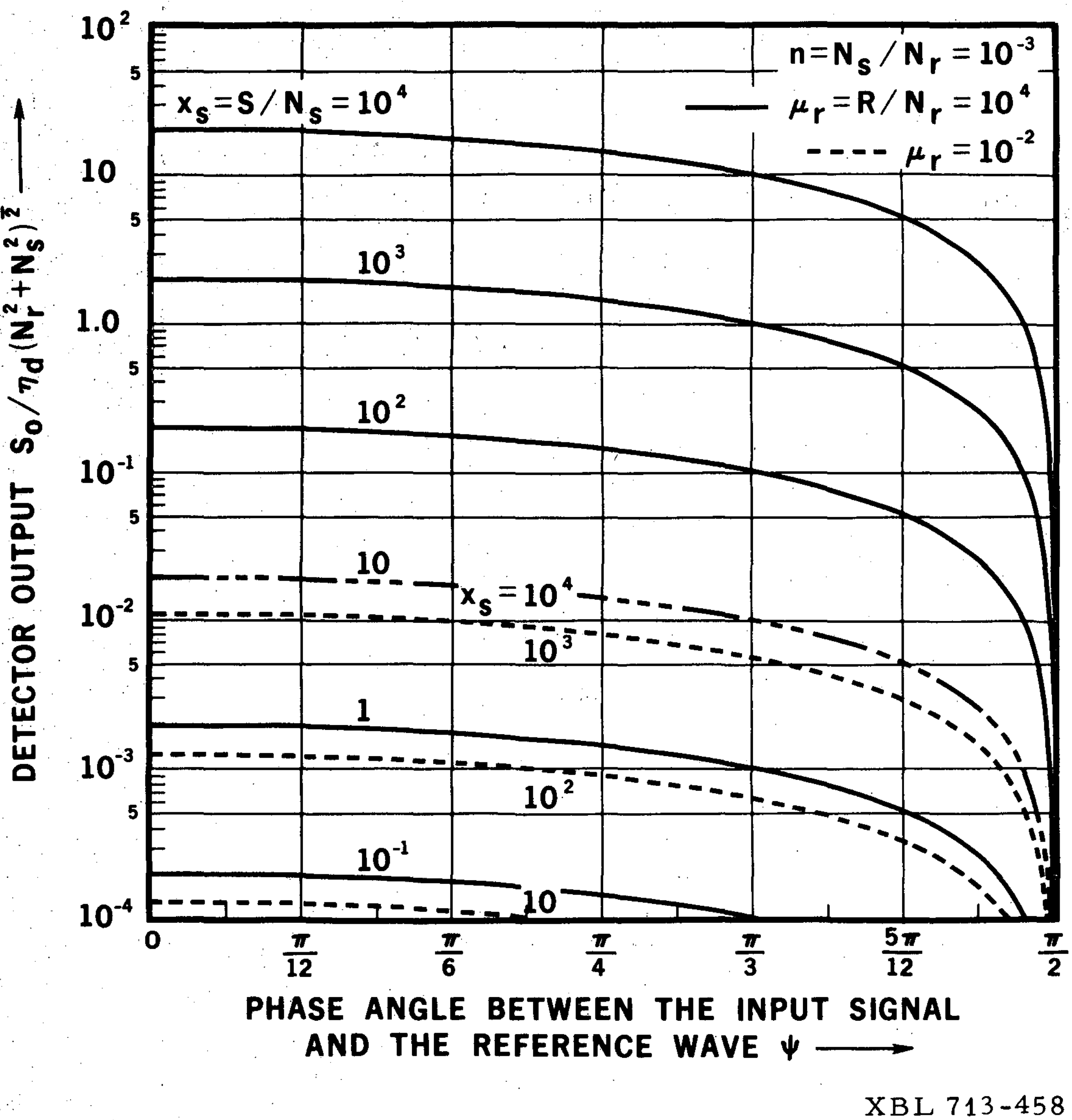

$n = N_s / N_r = 10^{-3}$
$\mu_r = R/N_r = 10^4$
$\mu_r = 10^{-2}$
$x_s = S/N_s = 10^4$
10^3
10^2
10
1
10^{-1}
$x_s = 10^4$
10^3
10^2
10
DETECTOR OUTPUT $S_o/\eta_d(N_r^2+N_s^2)^{\frac{1}{2}}$
PHASE ANGLE BETWEEN THE INPUT SIGNAL AND THE REFERENCE WAVE ψ
XBL 713-458

Fig. 7

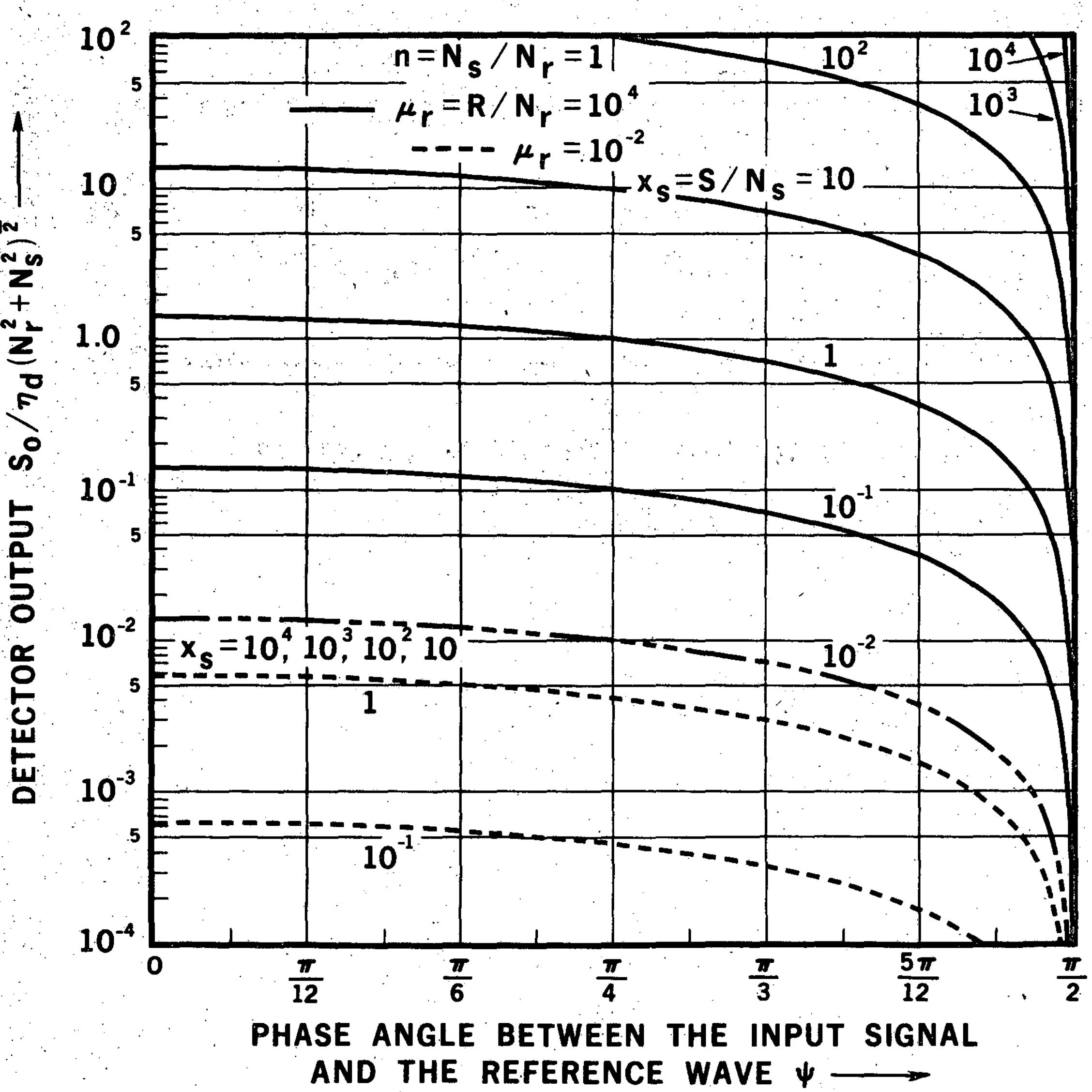

XBL 713-457

Fig. 8

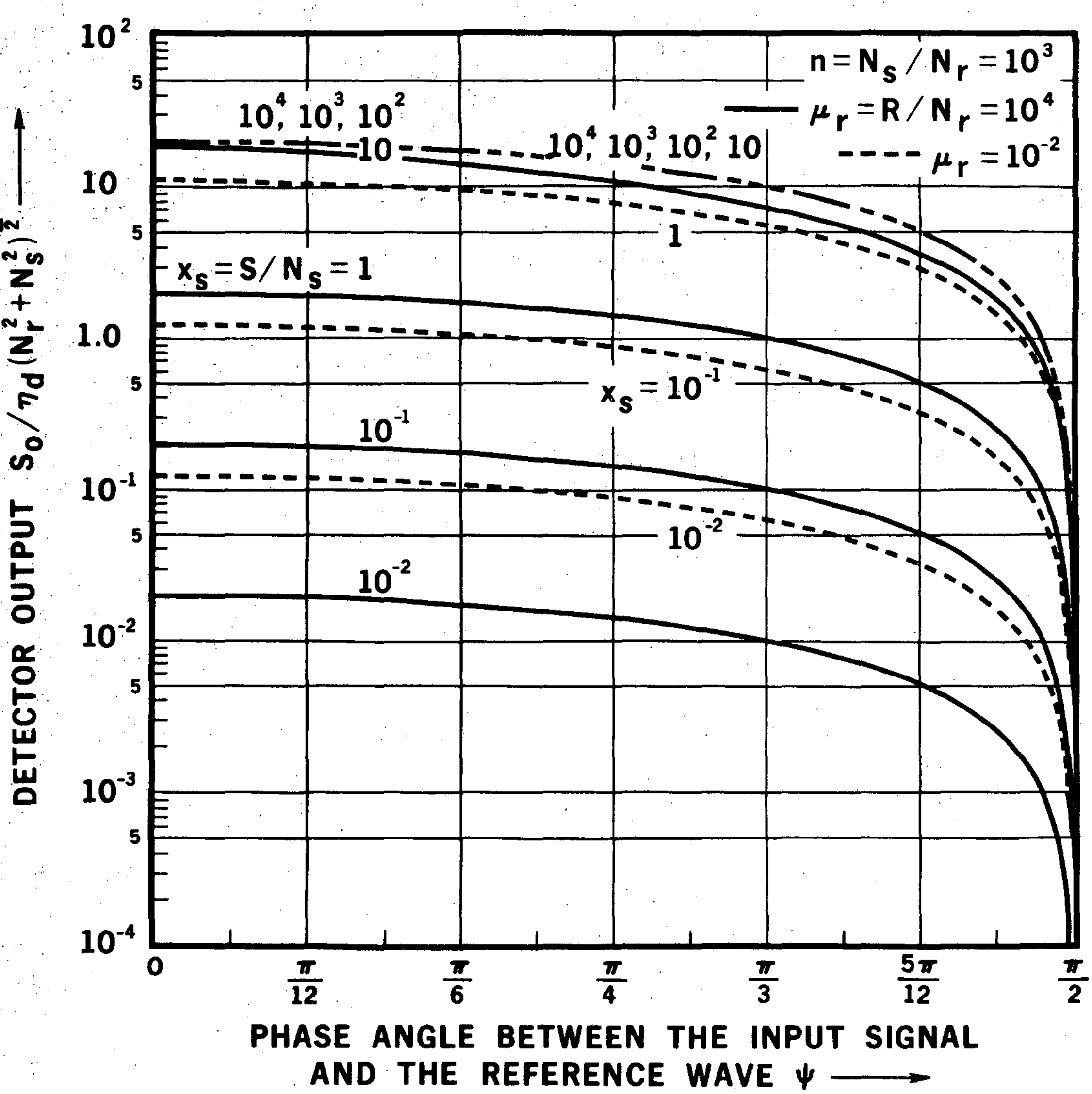

XBL 713-459

Fig. 9

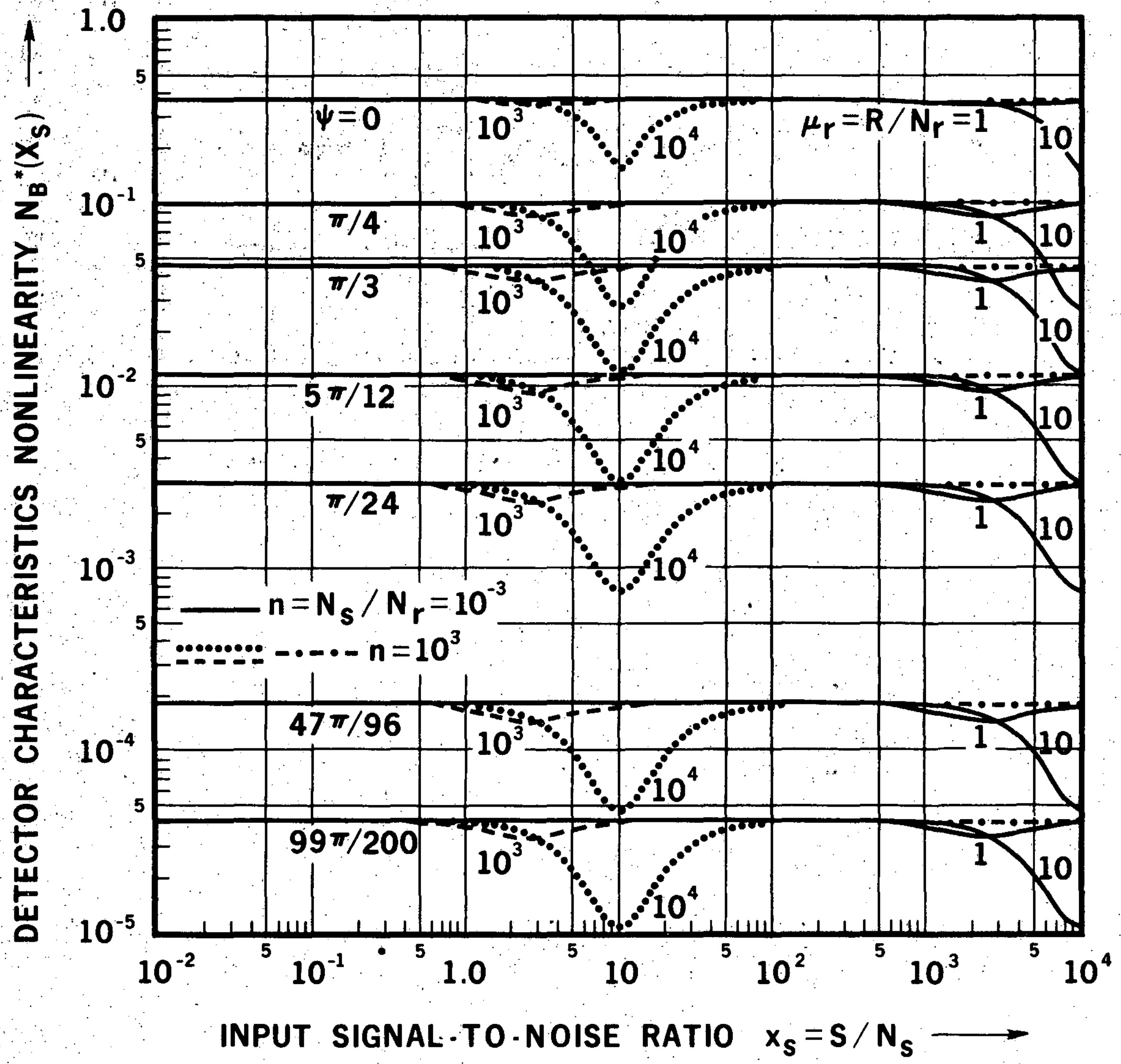

XBL 713-452

Fig. 10

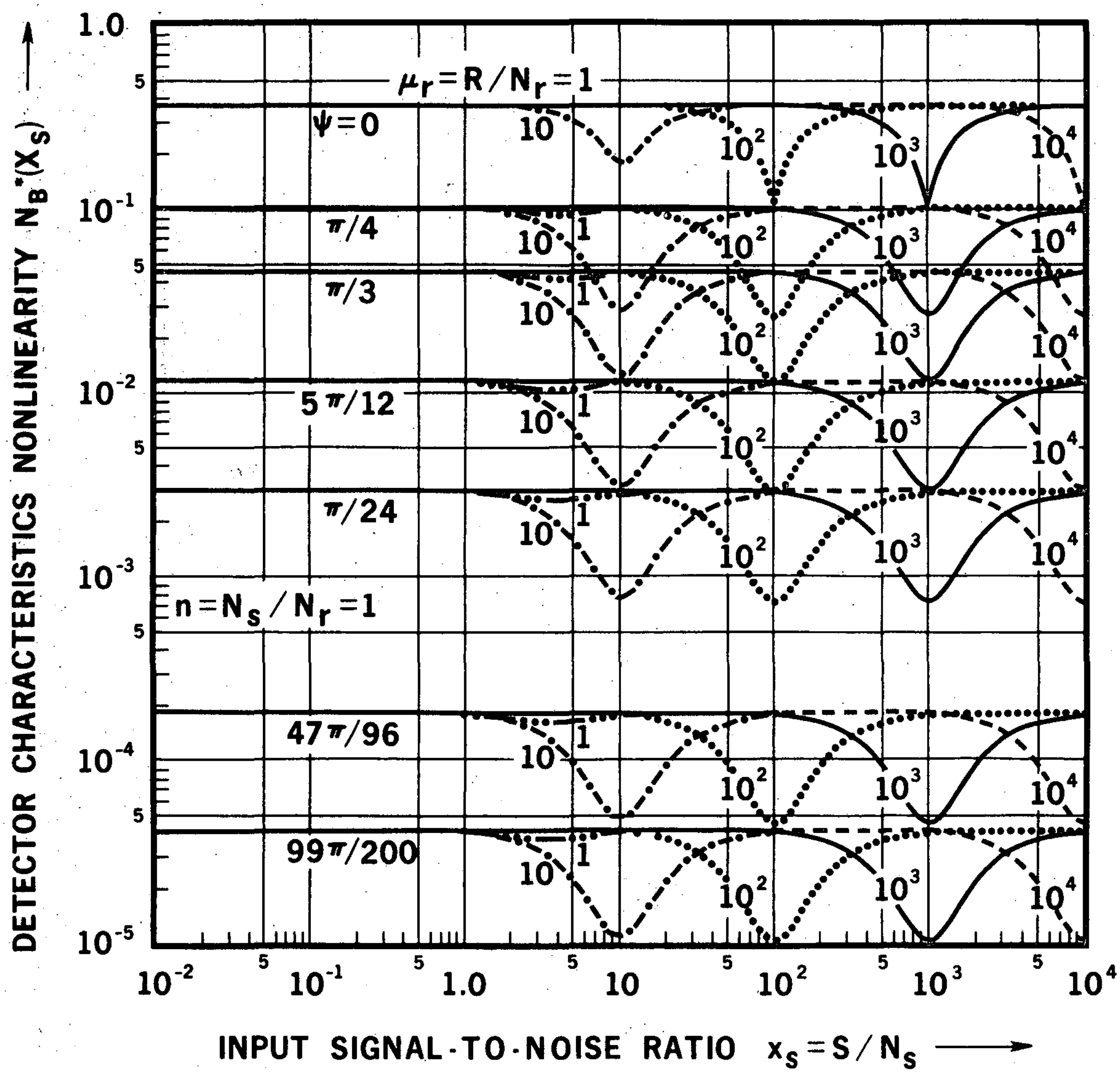

XBL 713-455

Fig. 11

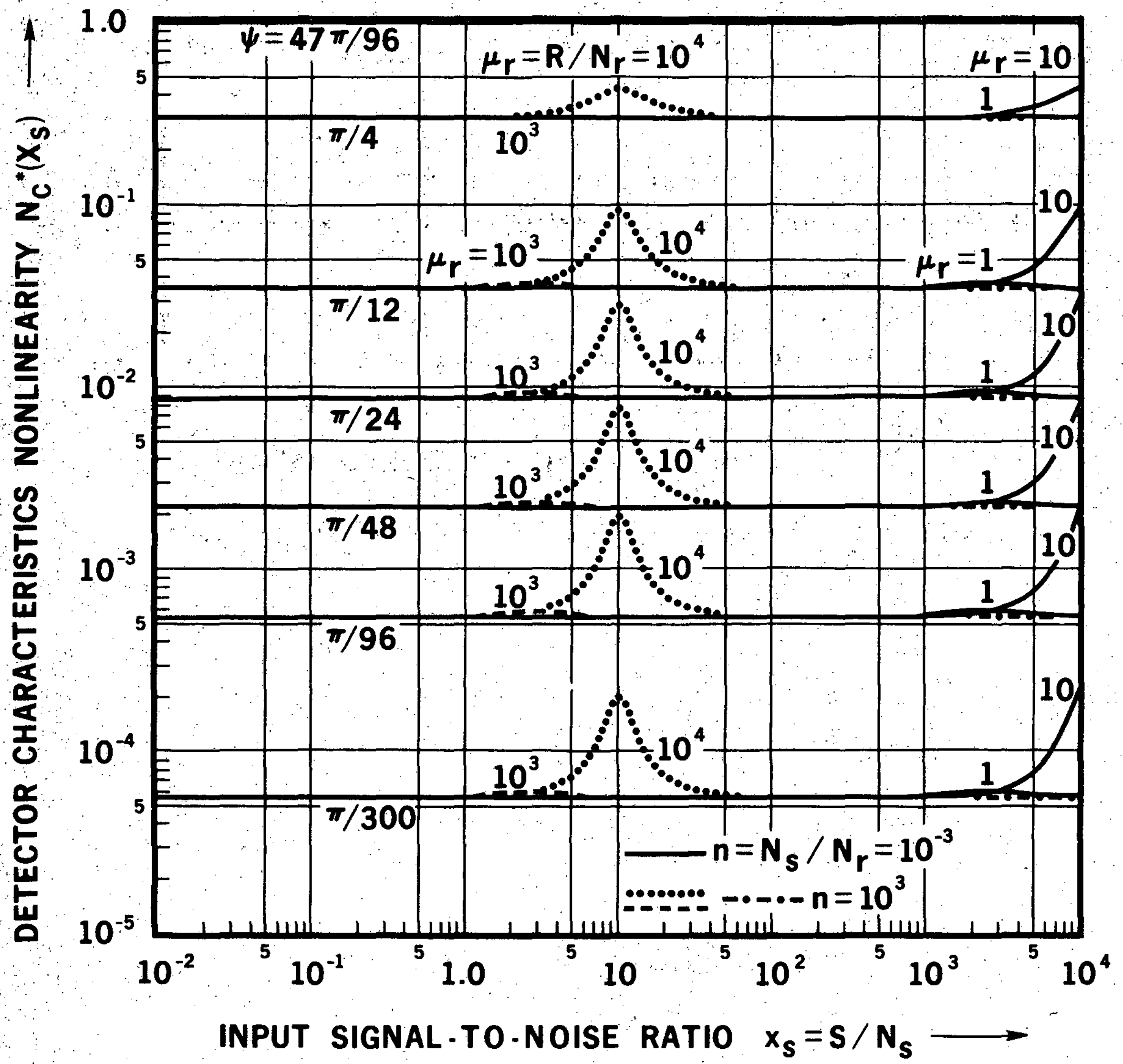

XBL 713-450

Fig. 12

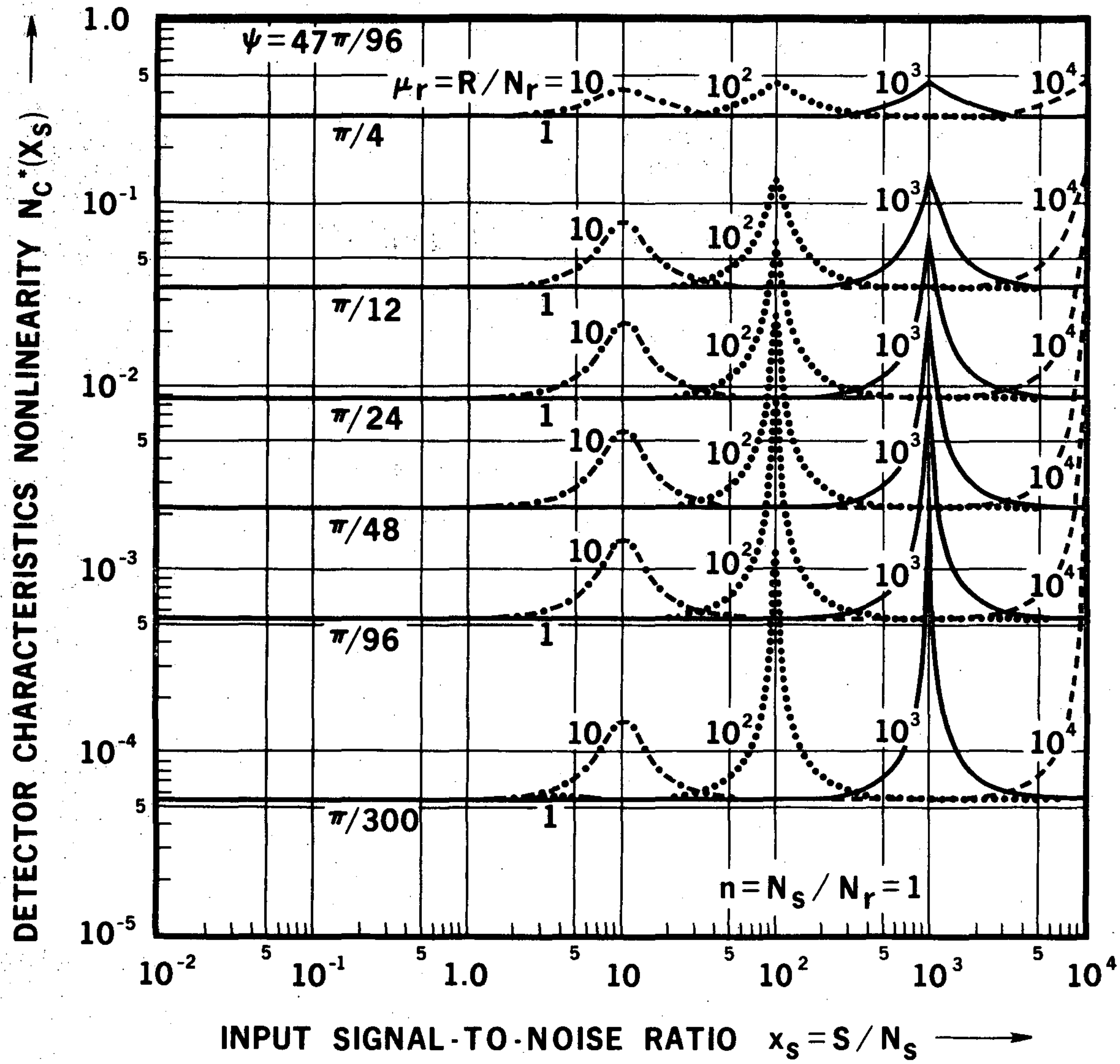

XBL 713-449

Fig. 13

TECHNICAL INFORMATION DIVISION
LAWRENCE RADIATION LABORATORY
UNIVERSITY OF CALIFORNIA
BERKELEY, CALIFORNIA 94720